

Assessment of a body force modeling approach to examine the aerodynamics of high bypass ratio fan stages

Original article

Jonas Grubert^{1,*}, Jens Friedrichs¹, Jan Göing¹

Article history:

Submission date: 11 December 2023

Acceptance date: 26 April 2024

Publication date: 12 August 2024

This is the updated version of a paper originally presented at the Global Power and Propulsion Technical Conference, GPPS Hong Kong 23, October 17–19, 2023.



*Correspondence:

JG: j.grubert@tu-braunschweig.de

Peer review:

Single blind

Copyright:

© 2024 Grubert et al. © This is an open access article distributed under the Creative Commons Attribution License (CC-BY 4.0), which permits unrestricted use, distribution, and reproduction in any medium, provided the original work is properly cited and its authors credited.

Keywords:

fan aerodynamics; reduced order model; body force modeling

Citation:

Grubert J., Friedrichs J., and Göing J. (2024). Assessment of a body force modeling approach to examine the aerodynamics of high bypass ratio fan stages. *Journal of the Global Power and Propulsion Society*. 8: 269–281. <https://doi.org/10.33737/jgpps/187995>

¹Institute of Jet Propulsion and Turbomachinery, Hermann-Blenk-Str. 37 38108 Braunschweig, Germany

Abstract

The primary focus of modern civil jet engine intake design is to enhance propulsive efficiency through an increase in the bypass ratio of the turbofan engine, which requires an enlargement in fan diameter. However, this enlargement results in increased weight and drag due to the need for a larger nacelle to surround the fan. To mitigate these issues, efforts are being made to shorten the axial length of the aircraft engine intakes. Nonetheless, this reduction leads to more vulnerable fan aerodynamics since the diffusion within the intake must occur over a shorter distance, causing a higher possibility of flow separation. Common intake design methods employ throughflow nacelle models that do not consider the aerodynamic effects of the fan, including blockage, mass flow redistribution, and suction. The utilization of a full annulus domain numerical setup, which is necessary to capture inlet distortions, demands excessive computational resources particularly during the design phase. As a result, reduced order models, such as the body force model, can be utilized to simulate fan intake aerodynamics. This paper will assess the body force model and its abilities by comparing conventional bladed single passage simulations with the body force approach.

Introduction

Further increasing the propulsor efficiency and decreasing the environmental impact of aviation is a challenging task, that requires ongoing research of new aircraft and especially propulsion technologies. Currently, there are a couple of promising development trends. On the one hand, fuselage- or wing-embedded propulsors show promising increases in efficiency, according to (Gunn and Hall, 2014) and (Uranga et al., 2017). On the other hand, further increases in the bypass ratio and decrease in fan pressure ratio of UHBR engines are also known to significantly improve the propulsor efficiency (Cumpsty, 2010). While boundary layer ingesting (BLI) propulsors inherently face the problem of asymmetric inlet conditions due to ingested boundary layers, asymmetric inlet conditions are of particular interest in the case of increasing bypass ratios. This is because this development trend requires a necessary reduction in inlet length to compensate for weight and drag losses that arise due to increasing bypass ratios (Peters, 2014). With decreasing fan pressure ratio, the fan becomes more susceptible to perturbations in the flow, thus making a reduction in inlet length even more critical, since flow separation is more likely to occur during operation with high angles of attack, e.g., maximum climb or crosswind conditions (Seddon and

Goldsmith, 1985). In both cases, it is important assess the performance of the fan and the components downstream under off design conditions as early as possible in a design cycle. However, full-annulus CFD simulations are necessary to capture the highly inhomogeneous flow that occurs during these off design conditions. However, such simulations require large amounts of computer resources, which is limiting during the early design phases. Reduced Order Models are a useful resource to consider the coupling between engine inlet and fan during the early design phases. In this paper the body force modeling (BFM) method will be assessed. This model uses source terms added to the Navier Stokes equations to represent the aerodynamic behavior of the blades in a circumferentially averaged manner without having to consider the blades spatially discretized, which significantly reduces the mesh size. This approach enables the steady simulation of a full-annulus fan stage within an intake under distorted inflow conditions - e.g. due to high angle of attack or crosswind - with drastically reduced computational cost.

First introduced by Marble (1964), the BFM approach was used in several studies. For example Gong et al. (1999) used the BFM approach for stall inception and distortion transfer, which was later used by Hsiao et al. (2001) to investigate the rotor's effect on inlet flow separation in a powered nacelle. Another field of application is the simulation of fan noise, which was done by Defoe et al. (2010). Peters (2014) used a modified version of Gong's model to build a design framework for ultra short nacelles for low fan pressure ratio propulsors. More recently Hall et al. (2017) proposed a new model formulation that eliminates the a priori calibration process necessary in earlier BFM applications making it even more suitable during early design phases. They validated the model's capabilities with experimental data by Gunn and Hall (2014). However, their proposed model did not include a loss model, but a diffusion factor to consider efficiency. This model has been modified by Thollet (2017) in order to make it viable for the application on transonic fan stages with a newly proposed loss model and metal blockage consideration. The main goal of the present paper is to evaluate a body force model, that is capable of resolving the aerodynamics of transonic fan stages. Therefore, the model by Thollet (2017) will be applied to a transonic fan stage and its results will be compared to conventional single passage simulations.

Methodology

The body force modeling approach replaces a physical blade row with an empty volume, in which a body force field is used to simulate the effects of the physical blades on the flow. This approach models the equivalent of the pitchwise averaged blade aerodynamics, as shown in Figure 1.

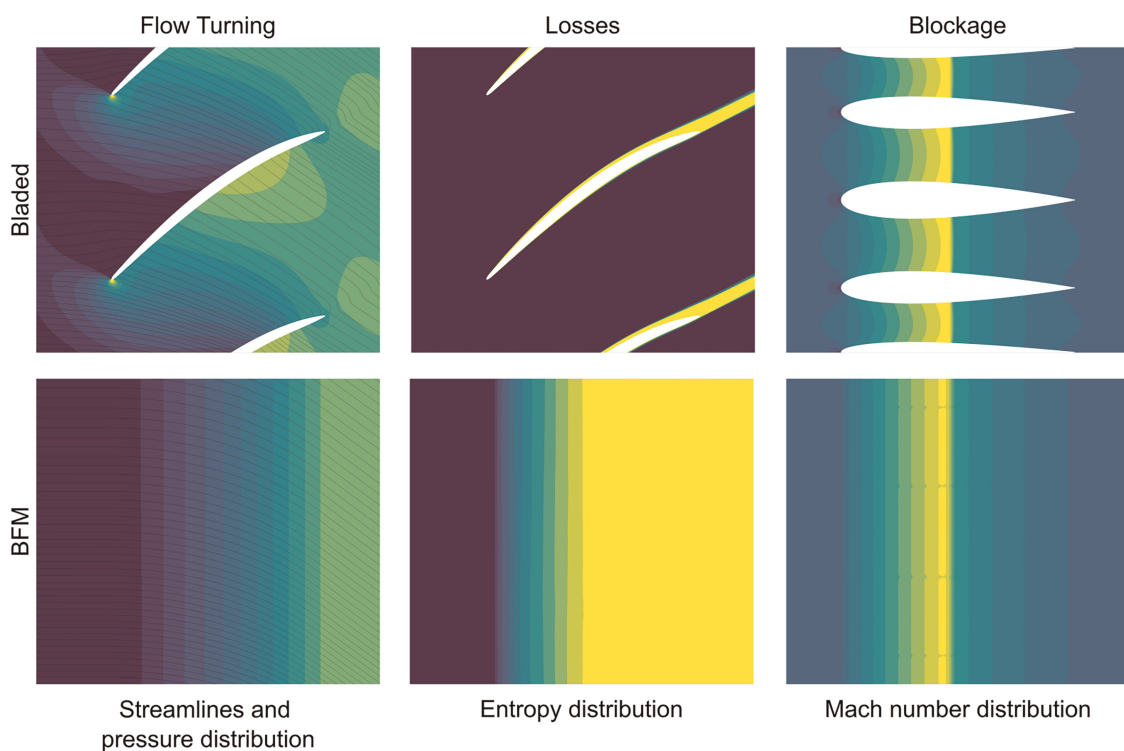


Figure 1. Body force modeling method.

While the approach is capable of producing similar flow turning and pressure rise, it does not capture local phenomena such as loss wakes, as can be seen in the contours of entropy. The modeling approach must account for the geometrical blockage caused by a physical blade row, as evident in the contours of Mach number in Figure 1.

The local body force f is calculated based on Equation (1),

$$f = \vec{f}_n + \vec{f}_p \tag{1}$$

where f_n represents the inviscid body force responsible for flow turning and inviscid work input, and f_p represents the viscous body force responsible for entropy generation and efficiency loss. Figure 2 illustrates the principle behind these two body force vectors. The inviscid body force always acts normal to the local streamline, while the viscous body force acts parallel to the local streamline against the direction of the flow. Therefore, the two vectors are referred to as the normal and parallel components of the body force, respectively.

Governing equations

The governing equations for the body force approach are those for mass (2), momentum (3) and energy conservation (4), (Liepmann, 2013):

$$\frac{\partial \rho}{\partial t} + \nabla \cdot (\rho V) = 0 \tag{2}$$

$$\frac{\partial}{\partial t}(\rho V) + \nabla \cdot (\rho V \times V) = -\nabla p + \nabla \cdot \tau + S_M \tag{3}$$

$$\frac{\partial \rho h_t}{\partial t} - \frac{\partial p}{\partial t} + \nabla \cdot (\rho V h_t) = \nabla \cdot (V \cdot \tau) + S_E \tag{4}$$

In the momentum equation the body force f gets added within the term $S_M = \rho f$. The same applies for the energy equation with $S_E = \rho f \cdot U$ where the blades rotation and thus its work input is represented by its blade velocity $U = \omega \cdot r$. In case of a stator there is no rotation, which means there is no work input $S_E = U = 0$.

Numerical setup

Due to the nature of the body force model, there is no circumferential variation in the model equations. The blade row gets modeled in an axisymmetric way. A comparison of the numerical setups of a bladed simulation versus a body force simulation is pictured in Figure 3.

Figure 3 illustrates a key advantage of the body force approach over traditional bladed domain simulations. In the bladed domain, it is necessary to have a high spatial discretization of boundary layers. On the other hand,

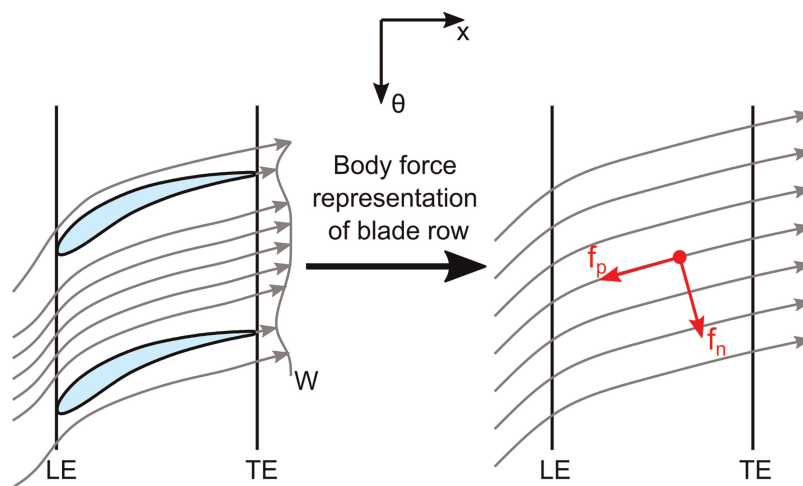


Figure 2. Relative flow through discrete blade passage (left) and relative flow through body force field (right). (Peters, 2014).

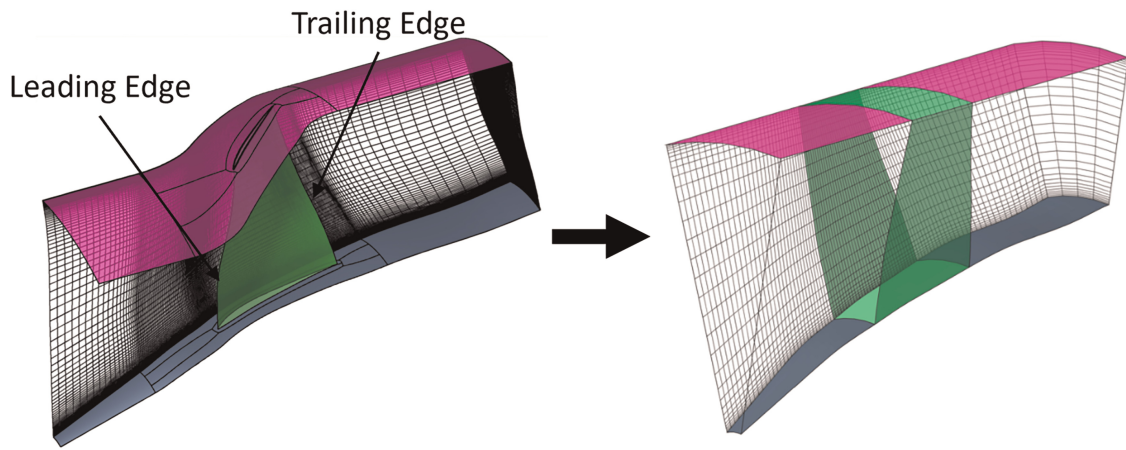


Figure 3. Comparison of numerical setups, Blade domain (left) and BFM domain (right).

the BFM domain can be spatially resolved much more coarsely, since there is no need to resolve the blade boundary layer. To create the mesh for the BFM domain, a 2D mesh is created in the meridional plane and then rotated in the circumferential direction, thus adding cells in the circumferential direction. This requires only information about the endwall geometry, as well as the location of the leading and trailing edge.

Unlike the axisymmetric nature of the BFM setup, the model can react locally to non-axisymmetric inflows. Therefore, the model is able to accurately simulate the effects due to inflow disturbances.

State of the art

The calculation of the two body force components \vec{f} can be achieved in several ways. Originally developed by Gong (1999), the formulation has undergone modifications over time. Recently, Hall et al. (2017) proposed a new formulation of the normal component, which only depends on local flow variables. This eliminates the need for empirical calibration, which was necessary in previous studies such as (Gong, 1999; Peters, 2014).

Hall's model uses the blade camber surface geometry as a priori input and can be expressed as follows:

$$f_n(x, r) = 2\pi\delta W^2 \frac{1}{s} \frac{1}{n_\theta} \quad (5)$$

The local inviscid body force is determined by equating the local deviation angle δ , local camber surface normal vector n_θ , relative flow velocity W and blade surface area, distributed over the local blade pitch s .

Although this model was capable of predicting the inviscid redistribution effect of a BLI propulsor, it could not predict efficiency, as Hall neglected the f_p component. Additionally, the model did not account for blockage effects, resulting in poorer performance for off-design conditions. However, Hall et al. (2017) and Akaydin and Pandya (2017) applied this model to several fan stages with inflow distortion for on-design conditions, demonstrating the model's capability to affordably and accurately represent fan stage aerodynamics with inflow distortion.

Further improvements were made by Thollet (2017) by

1. Adding a loss formulation in f_p to account for losses without any additional exterior input
2. Accounting for blockage effects
3. Correction for compressibility effects

Loss model

The main limitation of Hall's model was its inability to capture losses. Thollet uses a simple formulation which relies on the local friction coefficient C_f , which is derived from an empirical turbulent flat plate correlation and uses the local Reynolds number Re_x .

$$C_f = 0.0592 \cdot Re_x^{-0.2} \quad (6)$$

$$Re_x = \frac{\rho W_x}{\mu} \tag{7}$$

This leads to the loss fomulation:

$$f_p(x, r) = \frac{W^2}{2sb|n_\theta|} \left(2C_f + \underbrace{2\pi K_C (\delta - \delta^{\eta_{max}})^2}_{off-design-term} \right) \tag{8}$$

The off-design term in Equation (8) is determined using the distribution of the deviation angle $\delta^{\eta_{max}}(x, r)$ at peak efficiency. To estimate the performance at operating points away from peak efficiency, the local deviation distribution is compared to $\delta^{\eta_{max}}(x, r)$, controlling the slope of the compressor speedline towards stall and surge.

Blockage effects

In order to account for metal blockage effects and its influence on the choking mass flow, based on the reduction in effective flow area due to the presence of physical blades this has to be modeled within the body force approach. Therefore, a blockage factor b is introduced. The blockage factor b is a dimensionless factor that equates the camber to camber pitch distance s of two neighboring blades to the geometrical distance between pressure and suction side of these two blades. This parameter accounts for the reduction of effective area within a blade passage, as pictured in Figure 4.

It is calculated by

$$b = \frac{N_{Blades}(\theta_{SS} - \theta_{PS})}{2\pi} \tag{9}$$

The blockage factor is included within the governing Equations (2)–(4):

$$b \frac{\partial \rho}{\partial t} + \nabla \cdot (b\rho V) = 0 \tag{10}$$

$$\frac{\partial}{\partial t} (b\rho V) + \nabla \cdot (b\rho V \times V) = -b\nabla p + b\nabla \cdot \tau + bS_M \tag{11}$$

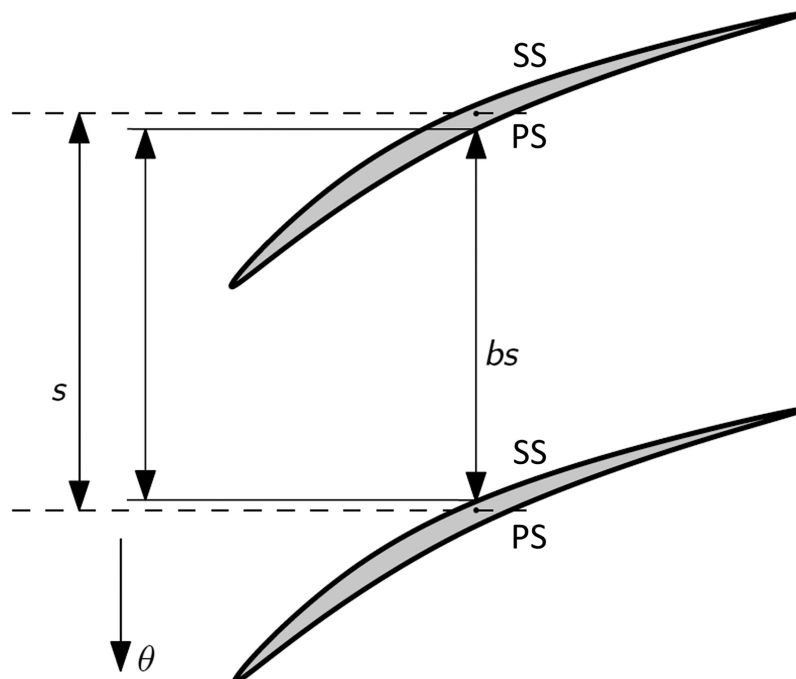


Figure 4. Definition of blade metal blockage parameter b .

$$b \frac{\partial \rho h_t}{\partial t} - b \frac{\partial p}{\partial t} + \nabla \cdot (b \rho V h_t) = \nabla \cdot (b V \cdot \tau) + b S_E \quad (12)$$

Compressibility correction

The original model by *Hall* was tested on incompressible test cases. *Thollet* has proven, that the following correction yields a valuable impact for transonic configurations. The baseline model of *Hall* is based on the lift coefficient of a thin airfoil at low Mach numbers, but the lift coefficient of an airfoil increases at high subsonic Mach numbers and has a different expression for supersonic flows. Therefore, a compressibility correction is added

$$K_C = \begin{cases} \min\left(\frac{1}{\sqrt{1 - Ma_r^2}}, 3\right), & Ma_r < 1 \\ \min\left(\frac{4}{2\pi\sqrt{Ma_r^2 - 1}}, 3\right), & Ma_r > 1 \end{cases} \quad (13)$$

which is an derivation of the Prandtl-Glauert correction for subsonic mach numbers and of the Ackeret formula for supersonic mach numbers. In order to avoid the singularity near $Ma = 1$, a blending function is used (*Thollet, 2017*).

Resulting equations

These modifications lead to the following model formulation for the inviscid and viscous body forces (*Thollet, 2017*):

$$f_n(x, r) = K_C \frac{W^2}{2} \frac{2\pi\delta}{sb|n_\theta|} \quad (14)$$

$$f_p(x, r) = \frac{W^2}{2sb|n_\theta|} (2C_f + 2\pi K_C (\delta - \delta^{\eta_{\max}})^2) \quad (15)$$

The necessary input for the model is the distribution of the metal angle $\kappa(x, r)$ and the blockage factor $b(x, r)$. the deviation angle distribution $\delta^{\eta_{\max}}(x, r)$ can either come from a first BFM simulation at peak efficiency or from a bladed simulation. This models capabilities will be discussed in the following and compared to a bladed model.

Implementation in solver

The results presented in this paper were obtained through the use of ANSYS CFX 21R2. ANSYS CFX uses a coupled solver, which solves the hydrodynamic equations as a single system with a fully implicit discretization of the equations (*ANSYS Inc, 2021*). In order to use the body force approach in CFX, it is necessary to divide the domain into several subdomains. The subdomains representing the rotor and stator have additional sources corresponding to f_n and f_p . These forces are added as *General Momentum Sources* to the momentum equation and as an additional Energy Source to the energy equation with $S_E = \omega r (f_n + f_p)$. The effects of metal blockage are accounted for, by making use of *porous domains* in CFX. In a porous domain, there is a virtual solid, that reduces the flow volume by limiting the volume V' available to flow in an infinitesimal control cell surrounding the point, and the physical volume V of the cell.

$$V' = \gamma \cdot V \quad (16)$$

Local blockage can be modeled, by defining a local volume porosity $\gamma(x, r)$ equal to the blockage factor $b(x, r)$.

Results and discussion

First, we discuss the blockage model and its performance in comparison to bladed simulations. Next, we evaluate the model's ability to predict compressor aerodynamics by using a transonic fan stage test case.

Blockage model

The blockage model was tested using a generic NACA0016 geometry (Eastman et al., 1933) as a stator. Since the geometry is a zero lift profile, there are no resulting inviscid body forces f_n since the blade is not cambered, thus resulting in $\kappa = 0$. Additionally, to differentiate the effect of the metal blockage, viscous forces were neglected. For turbulence closure, the $k-\omega$ -model by Wilcox (2008) is employed. The test case setup is shown in Figure 5(a). Figure 5(b) shows the associated distribution of the blockage factor $b(x, r)$.

The distribution in Figure 5(b) shows the geometric relationships for the blockage factor. Towards the leading and trailing edge the values of blockage factor approach $b = 1$. Close to the hub the values are the lowest because of the smallest circumferential distance between two neighboring blades while the distance towards the shroud increases due to the larger radius of the circle segment. A comparison of the body force approach against the bladed simulation is made in Figures 6 and 7.

Figures 6(a) and 6(c) illustrate the Mach number distribution for subsonic flow conditions. The axisymmetric nature of the body force model is evident in Figure 6(c), where no gradients in the Y direction are present. Both models accurately capture the flow acceleration in accordance with the Bernoulli equation, as demonstrated in Figure 7(a), where the circumferential averaged Mach number at midspan from inlet to outlet is compared. The BFM approach is capable of reproducing the magnitude, location, and slope of the Mach number peak, except for the onset of acceleration at the leading edge, which is not perfectly captured due to the missing stagnation point and its effect on the upstream flow in the BFM approach.

For transonic flow conditions, Figures 6(b), 6(d), and 7(b) depict the Mach number distribution. Similarly, the BFM approach accurately predicts the flow behavior, including the position of the shock and the faster flow downstream of the stator. However, the strength of the shock is underestimated, and the onset of acceleration at the leading edge of the stator is slightly underestimated as well.

These results demonstrate that the BFM approach, developed from Equations (10)–(12), can effectively capture metal blockage effects for the inviscid case. However, it should be noted that the validation of metal blockage has only been conducted for the inviscid case. For boundary layers due to viscous walls, the effective area between two neighboring blades decreases even more, which increases blockage due to aerodynamic effects. This aspect has not been addressed in this study but is left for future investigations. In addition, a relatively straightforward calculation was utilized to determine the blockage factor b . In previous studies, Baralon (2000) proposed an alternative approach to compute the blockage factor b . Unlike the approach adopted here, Baralon calculates the blockage factor perpendicular to the camber surface. Notably, Baralon was able to achieve encouraging results with the NASA 67 rotor. This approach is planned to be investigated further in future work.

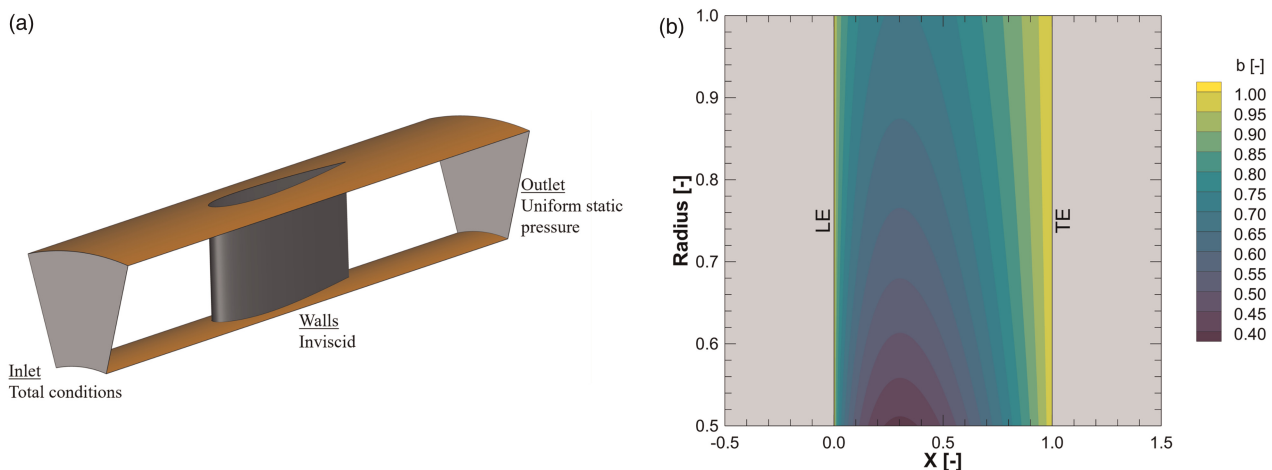


Figure 5. Stator test case. (a) Numerical setup of NACA0016 stator test case. (b) Blockage Factor distribution of NACA0016.

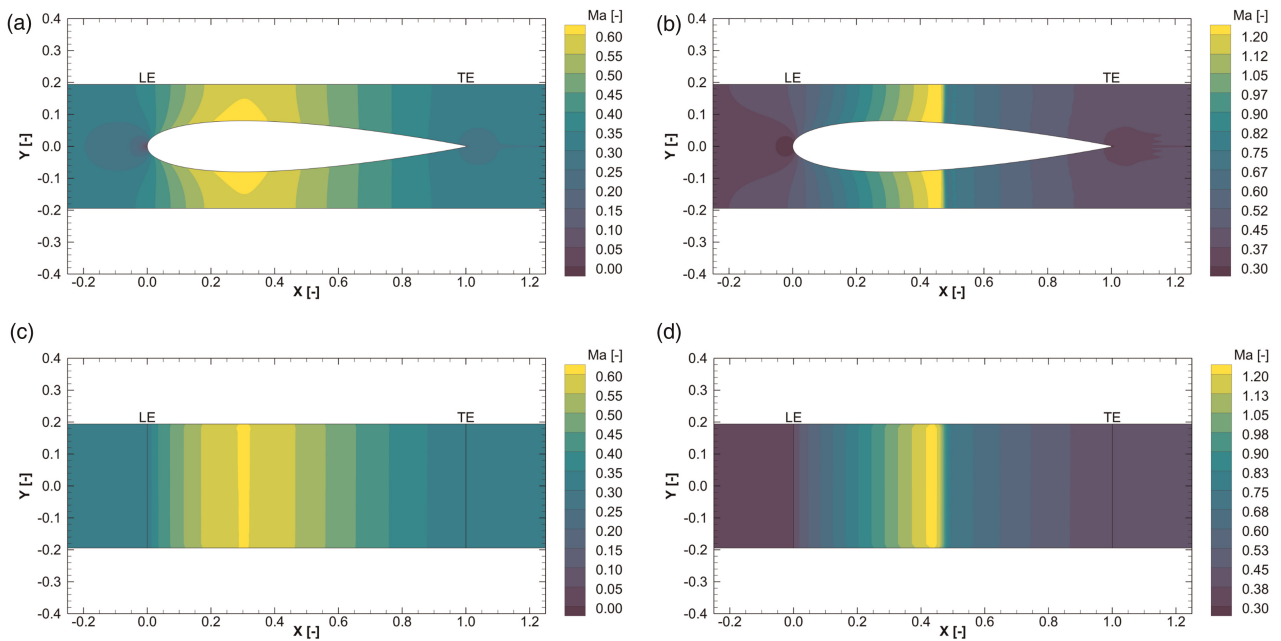


Figure 6. Contour plots of the Mach number at midspan for the NACA0016 stator test case. Subsonic conditions (left) and transsonic conditions (right). (a) Bladed Simulation with subsonic conditions. (b) Bladed Simulation with transsonic conditions. (c) BFM with subsonic conditions. (d) BFM with transsonic conditions.

Transsonic fan stage

In the following, the model is tested using a transonic fan stage. For this test case the CA3ViAR (Composite fan Aerodynamic, Aeroelastic, and Aeroacoustic Validation Rig) fan stage is used (Eggers et al., 2021) which features a composite low-transonic fan. Its fan stage characteristics are shown in Table 1.

To evaluate the accuracy of the model, a bladed simulation is conducted in conjunction with the BFM simulation. The numerical configurations for both simulations are displayed in Figure 8(b), with identical boundary conditions applied. The inlet is subjected to total conditions, while the outlet is maintained at a static pressure with radial equilibrium. With the exception of the horizontal hub in front of the spinner, all walls are assigned as viscous walls. For turbulence closure, the $k - \omega$ -model by Wilcox (2008) is employed. The bladed setup implements a mixing plane between the rotor and stator domains, which is unnecessary for the BFM setup. A comparison of the mesh statistics for both setups is presented in Table 2. The BFM setup has approximately one-fourth of the cell count of the single-passage bladed setup, and this can be further reduced since the BFM

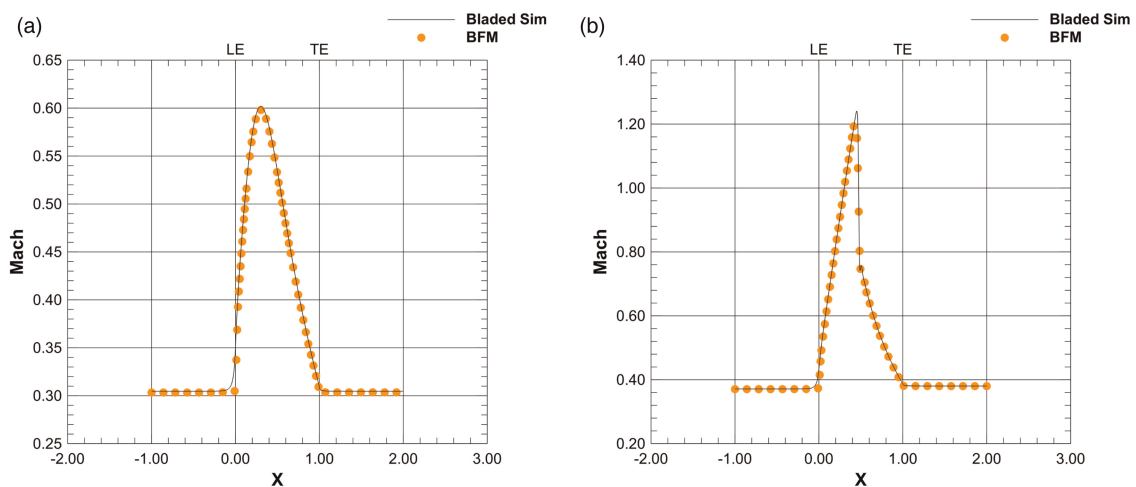


Figure 7. Circumferentially averaged Mach number at midspan from inlet to outlet for the NACA0016 stator test case. Subsonic conditions (left) and transsonic conditions (right). (a) BFM vs. Bladed Simulation with subsonic conditions. (b) BFM vs. Bladed Simulation with transsonic conditions.

Table 1. CA3ViAR fan stage characteristics.

Operating conditions			Cruise @ 0 km	Take-off @ 0 km
Bypass Ratio	α		17	17
Mach number	Ma_x		0.62	0.52
Poly. efficiency	η_{poly}		0.89	0.87
Total pressure ratio	π_t		1.37	1.32
Mass flow	\dot{m}	kg/s	63.39	57.15
Rot. speed	n	RPM	8,667	8,095
Fan tip speed	V_θ	m/s	295	275
Fan tip radius	r_{tip}	m	0.325	0.325
Fan tip clearance	$r_{clearance}$	mm	0.75	0.75
Hub-to-tip ratio	v		0.26	0.26

mesh has not been optimized yet. The primary objective of this study is to evaluate the precision of the BFM simulation in comparison to the bladed simulation, and mesh optimization will be considered in future work.

Figure 9 compares the results of bladed simulations and the body force approach for the *Cruise* and *T/O* operating points listed in Table 1. Speedlines were calculated for each operating point, and the total pressure rise over the fan $\pi_{t, fan}$ and the polytropic efficiency η_{poly} were plotted against the mass flow rate. The black line represents the bladed simulation data, the orange line represents the data obtained using the BFM approach, and the blue line represents the data obtained using the BFM approach without the off-design term in Equation (8).

The results demonstrate that the BFM approach accurately predicts the choke mass flow for both operating points. However, at lower mass flow rates, the BFM approach slightly overestimates the total pressure rise. The impact of the off-design term from Equation (8) can be observed by comparing the blue line to the orange line, which shows that the design term causes the slope of the speedline to decrease from the point of maximum efficiency towards lower mass flows. Without this term, the efficiency and work of the fan would be overpredicted by the BFM approach. However, even with the off-design term, Figure 9 shows that the efficiency is overpredicted by approximately 3% by the BFM approach. This overprediction decreases towards lower mass flow rates, which is consistent with the findings in (Thollet, 2017). The BFM approach currently cannot capture the effects of tip clearance present in the physical blade row. The model assumes no tip gap exists and adds work in this region, increasing the pressure ratio and polytropic efficiency.

Figure 10 presents the local result quality of the BFM approach, where the spanwise distributions of the work coefficient and isentropic efficiency downstream of the rotor are shown in Figure 10. These figures demonstrate

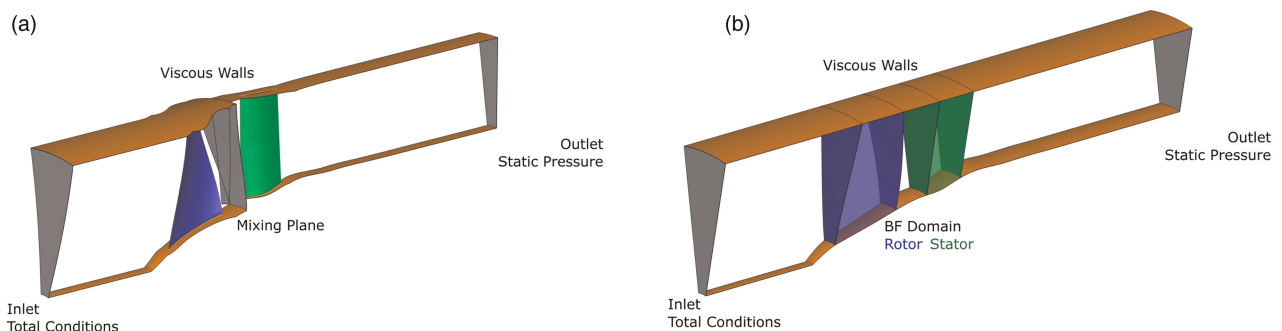


Figure 8. Numerical setups for CA3ViAR fan stage. (a) Bladed Simulation. (b) BFM.

Table 2. Mesh Statistics for the CA3ViAR Setup.

Mesh	Bladed Sim.	BFM
No. of Elements	3.747.456	1.039.300
Domain Size	1 Passage (1/18 Rotor and 1/40 Stator)	20° segment
y^+	< 2	> 10

that the BFM approach provides satisfactory results for the maximum efficiency operating point at the T/O operating condition. However, discrepancies in the model are evident in predicting the work input of the rotor accurately. The BFM overestimates the work input close to the hub and underestimates it in the direction towards the shroud, which is consistent with the findings in (Thollet, 2017). The lack of consideration of the tip gap does not justify this deviation. To further investigate this, a bladed simulation without a physical tip gap was performed, and the results are shown in the orange line. As expected, the absence of the peak gap increases the work input close to the shroud compared to the bladed simulation with a tip gap. However, this does not explain the spanwise distribution of the BFM approach. The isentropic efficiency in Figure 10 also shows similar behavior, where the BFM approach overestimates the isentropic efficiency near the hub and shroud but agrees precisely with the results in the core region of the flow.

Conclusions

In this study, a state-of-the-art body force model is considered to evaluate its ability to predict the aerodynamics of a transonic fan. To assess the model’s performance, the basic model was used along with modifications from the literature, and its blockage modeling functionality was validated using a simple stator test case. Following this, the model was applied to the CA3ViAR fan stage, where satisfactory results are obtained with one third of the mesh size compared to a bladed simulation. However, limitations of the model were also identified, which were previously documented in the literature.

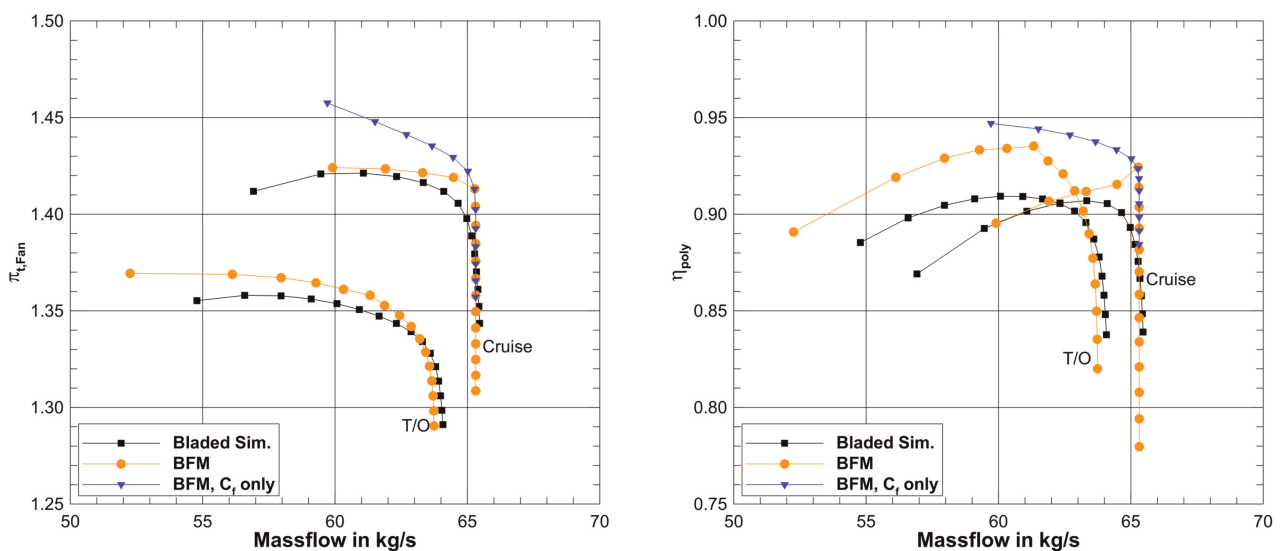


Figure 9. Compressor Map for the CA3ViAR fan stage test case, pressure ratio $\pi_{t,Fan}$ (left) and polytropic efficiency η_{poly} (right).

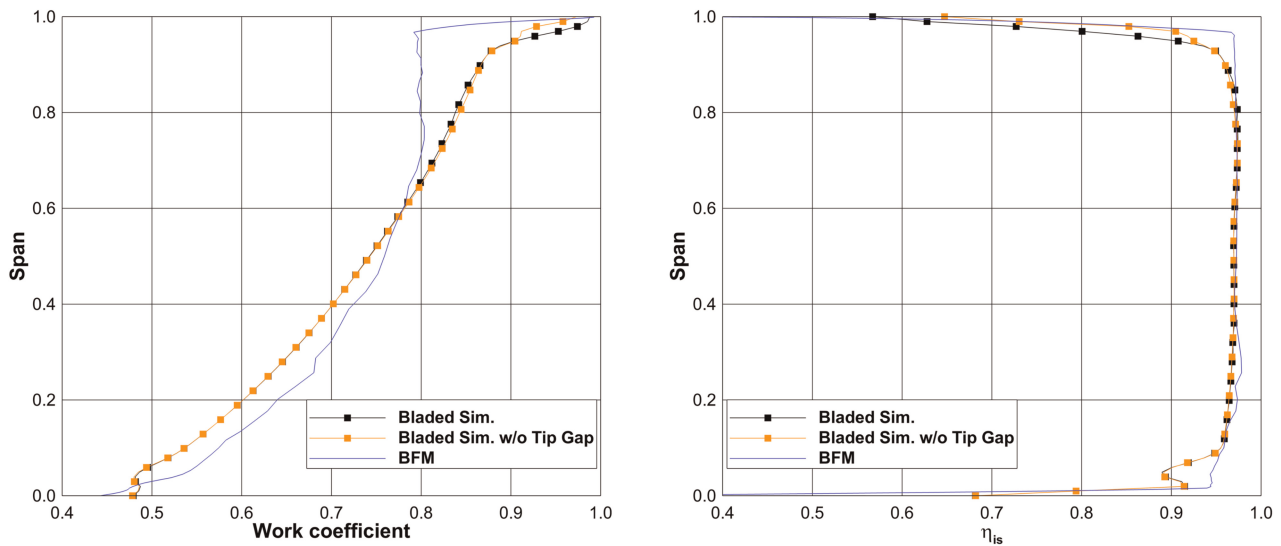


Figure 10. Spanwise profiles at peak efficiency for T/O conditions downstream of the rotor, Work coefficient (left) and isentropic efficiency (right).

Despite these shortcomings, the model serves as a valuable starting point for future modifications to improve its performance, particularly with respect to the tip gap aerodynamic. Previous works (Xie and Uranga, 2020, 2021), have attempted to modify the model, but the results are found to be insufficient for the transonic fan presented in this study. Thus, future research will focus on developing and testing new modifications to the model to address these limitations.

To validate the model, accompanying experiments will be performed using the INFRa rig (Grubert et al., 2022) at the Institute of Jet Propulsion and Turbomachinery. These experiments will not only investigate fan aerodynamics but also inlet distortion, which will be further studied in future work using the body force model. Overall, this study provides valuable insights into the capabilities and limitations of the body force model and highlights directions for future research.

Nomenclature

Latin

b	Blockage factor (–)
C_f	Local friction coefficient (–)
f	Body force per unit mass (m/s^2)
h	Enthalpy (J)
K_C	Compressibility correction factor (–)
Ma	Mach number (–)
N_{Blades}	Number of blades (–)
n_θ	Surface normal (–)
p	Pressure (Pa)
r	Radius (m)
Re_x	Local Reynolds number (–)
s	Pitch (m)
S_M	Momentum source ($\text{kg/m}^2\text{s}^2$)
S_E	Energy source (W/m^3)
t	Time (s)
V	Physical Volume (m^3)
V'	Virtual Volume (m^3)
W	Velocity (m/s)
x, y, z	Cartesian coordinates (m)

Greek

δ	Deviation angle (rad)
η	Efficiency (–)
γ	Volume porosity (–) Metal angle (rad)
μ	Dynamic viscosity (kg/m·s)
∇	Nabla operator (–)
ω	Angular velocity (rad/s)
ρ	Density (kg/m ³)
τ	Viscous stress tensor (–)
Θ	Angular direction (rad)

Indexes

<i>is</i>	Isentropic
<i>n</i>	Normal to local streamline
<i>p</i>	Parallel to local streamline
<i>poly</i>	Polytropic
<i>r</i>	Relative values
<i>t</i>	Total values
<i>x</i>	Local values

Abbreviations

BFM	Body Force Model
BLI	Boundary Layer Ingestion
LE	Leading Edge
NACA	National Advisory Committee for Aeronautics
NASA	National Aeronautics and Space Administration
MFR	Mass Flow Rate
PTF	Propulsion Test Facility
PS	Pressure Side
RANS	Reynolds Averaged-Navier Stokes
SS	Suction Side
TE	Trailing Edge
UHBR	Ultra High Bypass Ratio

Competing interests

Jonas Grubert declares that he has no conflict of interest. Jan Göing declares that he has no conflict of interest. Jens Friedrichs declares that he has no conflict of interest.

References

- Akaydin H. D. and Pandya S. A. (2017). Implementation of a body force model in overflow for propulsor simulations, In 35th AIAA Applied Aerodynamics Conference. American Institute of Aeronautics and Astronautics, p. 7.
- ANSYS Inc. (2021). *Ansys CFX-Solver Theory Guide*. Canonsburg, PA, USA: ANSYS Inc.
- Baralon S. (2000). *On Multistage Analysis of Transonic Compressors: From Axisymmetric Throughflow Time-Marching to Unsteady Three-Dimensional Methods: Zugl.: Göteborg, Chalmers Univ., Diss., 2000, Vol. N.S., 1602 of Doktorsavhandlingar vid Chalmers Tekniska Högskola*. Göteborg: Chalmers University of Technology.
- Cumpsty N. A. (2010). Preparing for the future: Reducing gas turbine environmental impact—igti scholar lecture. *Journal of Turbomachinery*. 132 (4): 8.
- Defoe J., Narkaj A., and Spakovszky Z. (2010). A body-force based methodology for predicting multiple-pure-tone noise: Validation. In 16th AIAA/CEAS Aeroacoustics Conference. American Institute of Aeronautics and Astronautics.
- Eastman J., Ward K., and Pinkerton R. (1933). The characteristics of 78 related airfoil sections from tests in the variable-density wind tunnel, *NACA Technical Report* (NACA-TR-460).
- Eggers T., Friedrichs J., Goessling J., Seume J. R., Natale N., et al. (2021). Composite uhbr fan for forced response and flutter investigations. In Proceedings of ASME Turbo Expo 2021: Turbomachinery Technical Conference and Exposition. The American Society of Mechanical Engineers.

- Gong Y. (1999). A Computational Model for Rotating Stall and Inlet Distortions in Multistage Compressors. PhD thesis, Massachusetts Institute of Technology, Cambridge.
- Gong Y., Tan C. S., Gordon K. A., and Greitzer E. M. (1999). A computational model for short-wavelength stall inception and development in multistage compressors. *Journal of Turbomachinery*. 121 (4): 726–734. <https://doi.org/doi:10.1115/1.2836726>.
- Grubert J., Brunow P., Friedrichs J., Winkelmann P., Meillard L., et al. (2022). Design and development of a combined intake fan test rig to enable investigations of stable operating ranges. *ISABE-2022-207*.
- Gunn E. J. and Hall C. A. (2014). Aerodynamics of boundary layer ingesting fans. In Proceedings of the ASME Turbo Expo: Turbine Technical Conference and Exposition – 2014, edited by H. Hodson. ASME.
- Hall D. K., Greitzer E. M., and Tan C. S. (2017). Analysis of fan stage conceptual design attributes for boundary layer ingestion. *Journal of Turbomachinery*. 139 (7): 74.
- Hsiao E., Naimi M., Lewis J. P., Dalbey K., Gong Y., and Tan C. (2001). Actuator duct model of turbomachinery components for powered-nacelle navier-stokes calculations. *Journal of Propulsion and Power*. 17 (4): 919–927. <https://doi.org/doi:10.2514/2.5825>.
- Liepmann H. W. (2013). *Elements of Gas Dynamics*. Dover Books on Aeronautical Engineering, Dover Publ, Mineola, NY.
- Marble F. E. (1964). Section C. three-dimensional flow in turbomachines. In: Aerodynamics of Turbines and Compressors. (HSA-1), edited by W. R. Hawthorne. Princeton: Princeton University Press, pp. 83–166.
- Peters A. (2014). Ultra-Short Nacelles for Low Fan Pressure Ratio Propulsors. PhD thesis, Massachusetts Institute of Technology, Cambridge.
- Seddon J. and Goldsmith E. L. (1985). *Intake Aerodynamics: An account of the mechanics of flow in and around the air intakes of turbine-engined and ramjet aircraft and missiles*. London: Collins.
- Thollet W. (2017). Body Force Modeling of Fan-Airframe Interactions. PhD thesis, ISAE-SUPAERO, Toulouse, France.
- Uranga A., Drela M., Greitzer E. M., Hall D. K., Titchener N. A., et al. (2017). Boundary layer ingestion benefit of the d8 transport aircraft. *AIAA Journal*. 55 (11): 3693–3708. <https://doi.org/doi:10.2514/1.J055755>.
- Wilcox D. C. (2008). Formulation of the k-w turbulence model revisited. *AIAA Journal*. 46 (11): 2823–2838. <https://doi.org/doi:10.2514/1.36541>.
- Xie T. and Uranga A. (2020). Development and validation of non-axisymmetric body-force propulsor model. In AIAA Propulsion and Energy 2020 Forum. American Institute of Aeronautics and Astronautics.
- Xie T. and Uranga A. (2021). Capturing aero-propulsive coupling effects with a body-force propulsor model. In AIAA Propulsion and Energy 2021 Forum. American Institute of Aeronautics and Astronautics.